Curium(III) and europium(III) as luminescence probes for plant cell (Brassica napus) interactions with potentially toxic metals

Moll, H.; Schmidt, M.; Sachs, S.;

Originally published:

January 2021

Journal of Hazardous Materials 412(2021), 125251

DOI: https://doi.org/10.1016/j.jhazmat.2021.125251

Perma-Link to Publication Repository of HZDR:

https://www.hzdr.de/publications/Publ-31695

Curium(III) and europium(III) as luminescence probes for plant cell (*Brassica napus*) interactions with potentially toxic metals

Henry Moll[*a], Moritz Schmidt[a], Susanne Sachs[a]

[a] *Helmholtz-Zentrum Dresden-Rossendorf, Institute of Resource Ecology, Bautzner Landstraße 400, 01328 Dresden, Germany*

Abstract

We have investigated the interaction of the actinide Cm(III) and its lanthanide homologue Eu(III) with cells of *Brassica napus* in suspension. This study combines biochemical techniques (plant cell response) with spectroscopic experiments to determine the chemical speciation of hazardous metals in contact with the plant cells. Experiments conducted over a period of 7 d showed that *B. napus* cells were able to bioassociate both potentially toxic metals in significant amounts up to 0.58 µmol Eu/$g_{\text{fresh cells}}$ and 1.82 µmol Cm/$g_{\text{fresh cells}}$ at 30 µM Eu(III) and 0.68 µM Cm(III), respectively. For Cm(III), a biosorption process could be identified as soon as 5 h post-exposure with 73±4% of the Cm(III) bioassociated. Luminescence spectroscopy results based on UV and site-selective excitation confirmed the existence of three Cm(III)/Eu(III) [M(III)] species in both the supernatants and cells. The findings detailed herein support that M(III) coordinates to two kinds of carboxyl groups and phosphate groups.

Keywords: actinides; lanthanides; plant cells; laser spectroscopy; speciation

[*] Address correspondence to Henry Moll, Institute of Resource Ecology, Helmholtz-Zentrum Dresden-Rossendorf, Bautzner Landstrasse 400, 01328 Dresden, Germany. E-mail: h.moll@hzdr.de.

1. Introduction

Hazardous elements such as radionuclides (RN) dispersed in the environment pose a safety risk for the biosphere. As such, their migration and transfer behaviors must be determined prior to undertaking a reliable risk assessment of these potentially harmful substances. It is well known that RN can be introduced into the animal and human food chains via soil-plant pathways (Schulz and Ruggieri, 1981). For instance, nuclear weapons testing and nuclear power plant (NPP) accidents (e.g., Chernobyl and Fukushima) have been linked to the release of RN into the environment, among those Pu, Am, and Eu isotopes. Moreover, in the case of nuclear waste repositories, incident scenarios such as the ingress of water may lead to the unwanted release of actinides (e.g., U, Pu, Am, Cm) and their transport into the environment. Am is a trivalent radioelement of particular concern; for instance, ^{241}Am is significantly more toxic and mobile than ^{241}Pu. A recent study indicates that approximately 1.5×10^{14} Bq of ^{241}Am, resulting from the beta-decay of about 6×10^{15} Bq of ^{241}Pu, was released into the near-surface environment as a result of the 1986 Chernobyl NPP accident (Thakur and Ward, 2019). Indeed, 90% of these α-emitting nuclides tend to be located at depths of 5-10 cm (Bondar'kov et al., 2006), making them available for uptake via plant roots. Eu(III) and Cm(III) can be used to mimic the behavior of Am(III) in plant cells (e.g. Ansoborlo et al., 2006; Ménétrier et al., 2008). While plants can accumulate both essential and non-essential metals in their tissues, they are not able to distinguish between metals with similar physicochemical properties (e.g. Ca(II) and Cm(III)) or between two isotopes of the same metal (Sharma et al., 2015).

Also important to this discussion is the growing use of lanthanides for a variety of scientific and industrial products. However, the challenge of extracting lanthanides in usable quantities, coupled with subsequent processing methods, can also lead to the unwanted release of these potentially hazardous elements into the environment. Lanthanides and actinides display many similarities based on their comparable ionic radii for elements of the same oxidation state and their analogous aqueous chemistry; hence, lanthanides are considered to be suitable chemical analogs for actinides from a (bio-)chemical point of view (Ansoborlo et al., 2006). For instance, Drake et al. used lanthanide ion probe spectroscopy in order to characterize the Eu^{3+} binding sites on *Datura innoxia* cell wall fragments (Drake at al., 1997). Using time-resolved laser-induced fluorescence spectroscopy (TRLFS), Fellows et al. confirmed Eu(III) uptake in oat (*Avena sativa*) roots, as well as the preferential uptake of Eu(III) within undifferentiated root cells as a strong inner-sphere mononuclear Eu(III) complex (Fellows et al., 2003). However, there are only a few

reports of the impact of rare earth elements (REE)/lanthanides in biological systems (e.g. Martinez-Gomez and Skovran, 2016). For instance, the replacement of Ca(II) by REE in tissues and enzymes, as well as the influence on the Ca(II) influx in cells, has been reported in the literature (e.g. Lin et al., 2006). In contrast, much still has to be learned about the influence of Cm(III) on plant cell metabolism. Earlier studies (using, for example, lysimeter measurements) demonstrated the uptake of Cm(III) from contaminated soil in a range of different plants. Bahia grass, clover, corn, soy bean, and wheat grown in contaminated soil accumulated ~1.5% of the available ^{244}Cm (Adriano et al., 1981). The uptake and translocation of ^{237}Np, ^{238}Pu, $^{239/240}$Pu, ^{241}Am, and ^{244}Cm into selected plants (alfalfa, barley, peas, cheat grass, and wheat) have been reported (Schulz and Ruggieri, 1981; Schreckhise and Cline, 1980), with ^{244}Cm uptake about 10-20 times higher than Pu. Further investigations into the translocation of ^{244}Cm confirmed that ^{244}Cm levels were 30 to 50 times lower in barley seeds compared to the entire plant. For wheat, only 0.1% of ^{244}Cm was identified within the grain itself, while 52% of the ^{244}Cm was located in the lower half of the stem and leaves. It should also be noted that the wheat plant could not distinguish between ^{241}Am and ^{244}Cm. To the best of our knowledge, no spectroscopic speciation analyses of Cm(III) in the presence of plants or plant cells have been reported thus far.

Since actinides and lanthanides such as Cm(III) and Eu(III) are non-essential elements, they are unlikely to have a specific route for transport into plants. Nonetheless, they can be taken up by plants and may interfere with normal metabolic processes. In our previous studies, we demonstrated the significant potential of *B. napus* cells (callus and suspension cell cultures) to bioassociate Eu(III) and U(VI) due to the interaction of both metals with cell walls and cell surface structures (Moll et al., 2020a; Jessat et al., 2021). Laurette et al. reported that *B. napus* can accumulate heavy metals in higher quantities than many other species (Laurette at al., 2012).

Unspecialized plant cells can serve as useful models for studying the physiological and biochemical response mechanisms toward a number of stress factors at the cellular level (Huang et al., 2017a; Zagoskina et al., 2007; Rajabi et al., 2021). Various studies have confirmed that plant cells do respond to heavy metal stress (e.g., Cd, Tb, and U) with an increased concentration of intracellular Ca (Küpper and Kochian, 2010; Huang et al., 2020b; Cao et al., 2018; Yang et al., 2015; Rajabi et al., 2021). There is currently a lack of knowledge on the interaction of plant cell cultures with trivalent actinides with regard to their bioassociation, distribution, and Ca(II)/Mg(II) homeostasis; moreover, their impact on cell growth and

metabolism also remains poorly understood. Additionally, the speciation of trivalent actinides and lanthanides in plant cells and their cell compartments has yet to be fully investigated.

Cm(III) and Eu(III) have been used as molecular probes to explore their speciation behaviors on or in suspension cells and supernatants. TRLFS based on UV and site-selective excitation represent non-invasive, selective, and highly sensitive methods for detecting Cm(III) and Eu(III) in the nM to µM concentration range, with resulting spectroscopic data used to determine the local environment of either metal (Edelstein et al., 2006; Binnemans, 2015). However, the ability to accurately discriminate multiple M(III) species after UV excitation at 394.0 and 396.6 nm, respectively can be hampered by the simultaneous excitation of all present species. This limitation can be addressed by utilizing site-selective luminescence spectroscopy, which has been demonstrated to be a very useful tool for characterizing samples containing M(III) in multiple environments (Schmidt et al., 2008; Johnstone et al., 2016; Wolter et al., 2019). Excitation of Eu(III)'s $^5D_0 \rightarrow {}^7F_0$ transition yields a single peak for each respective species due to the non-degeneracy of electronic states with J = 0 (Görller-Walrand and Binnemans, 1996). Subsequent direct excitation of the identified species facilitates the acquisition of detailed information on the local coordination symmetry of Eu from characteristic emission band splittings; this approach can also aid in determining the number of water molecules for the different species from luminescence decay lifetime data.

For this study we expanded our approach published in (Moll et al., 2020a) to identify differences between interactions of callus cells and cell suspensions, with a focus on Cm(III) as a representative of the trivalent actinides. Furthermore, this study was also designed to address the effects of the cell mass-to-metal ratio over a wide range; specifically, metal concentrations were varied from 0.7 – 200 µM, while cell mass ranged between 40 – 600 g/L. We also utilized spectroscopic analysis, both in suspension and for the first time by applying site-selective TRLFS, to identify the functional groups responsible for M(III) binding in a biological system. All results discussed herein focus on the long-term behavior of the cells.

2. Materials and methods

2.1. Cell cultivation and Eu(III)/Cm(III) interaction experiments

To obtain suspension cell cultures, *B. napus* callus cells (PC-1113, DSMZ Braunschweig, Germany) were transferred to a modified liquid Linsmaier and Skoog medium R, pH 5.8 (Linsmaier and Skoog, 1965), as described by Sachs et al. (Sachs et al., 2017). Cell cultivation was carried out on an orbital shaker (Model

SM-30, Edmund Bühler GmbH, Bodelshausen, Germany) at room temperature. For Eu(III) exposure experiments, the cells were grown in medium R with a reduced phosphate concentration of 6.25×10^{-6} M (medium R_{red}, Tab. SI1). The original phosphate concentration of the medium was reduced to minimize the precipitation of Eu(III). One week before Eu(III) addition, 0.4 or 6 g wet cells were transferred into Erlenmeyer flasks. 10 mL medium R_{red} was added to each flask to adapt the cells to this medium. After the adaption period, the cell culture medium was removed and 10 mL of fresh medium R_{red} was added. Subsequently, aliquots of a sterile 0.01925 M $EuCl_3$ stock solution (99.999%, Aldrich, Taufkirchen, Germany) were added to obtain final Eu(III) concentrations of 30 or 200 µM (cf. Table 1). Control cells were cultivated under the same conditions without the addition of Eu(III). Cell exposure was carried out on a horizontal shaker with slight agitation at room temperature. The exposure time was fixed at 7 d. The pH value of the cell culture media was measured at the end of the experiments (pH meter pH720, WTW inolab, Weilheim, Germany; with a Blue Line 16 pH electrode, SI Analytics, Mainz, Germany). The pH fluctuations ranged from 5.2 to 6.2. After exposure, the cells were separated from the media. The supernatants were centrifuged (11,000 rpm, room temperature; centrifuge 5804R, Eppendorf, Hamburg, Germany) and inductively coupled plasma-mass spectrometry (ICP-MS; Models NexION 350x, Perkin Elmer, Rodgau, Germany and iCapRQ, Thermo Fisher Scientific, Waltham, Massachusetts, USA) measurements were performed to determine the concentration of Eu(III) in the medium before and after cell exposure. After separation, the cells were washed with 10 mL 0.154 M NaCl solution at pH 5.8, after which cell vitality was measured (see Supplementary Information section). The Eu(III) speciation in medium R_{red} is discussed in the Supplementary Information section (cf. Table SI2 and Fig. S9). For each cell concentration measurement, a total of four independent experiments were performed.

Cell digestion experiments were performed as described in our prior work (Moll et al., 2020a), in order to determine the amount of the Mg(II) and Ca(II) content in the cells. The results represent mean values and standard errors (SE) of the mean.

Solutions with model compounds including phosphate, oxalic acid, phytic acid, phosphoenolpyruvate, malonic acid, citric acid, maleic acid, and p-coumaric acid with 30 µM Eu(III) in 0.154 M NaCl at pH 5.8 were prepared for TRLFS measurements. The ligand concentration was set to 30, 60, and 90 µM.

For experiments with Cm(III), 265±20 mg *B. napus* callus cells were transferred into 15 mL Greiner tubes (Greiner, Bio-one, Frickenhausen, Germany). The cells were suspended in 4 mL 0.154 M NaCl with a pH of 5.8 (cf. Table 1).

Table 1: Sample classification.

[Cells] (g/L)	$[M^{3+}]$ (µM)			
	0.68	2	30	200
40			Eu03040-S, Eu03040-C	Eu20040-S, Eu20040-C
66	Cm000766-S, Cm000766-C			
69		Cm00269-S, Cm00269-C		
600			Eu030600-S, Eu030600-C	Eu200600-S, Eu200600-C

S: supernatant, C: cells.

For site-selective experiments with Cm(III), 830 mg *B. napus* callus cells were transferred into 15 mL Greiner tubes. The cells were suspended in 12 mL 0.154 M NaCl with a pH of 5.8. The tubes were transferred in a glove box under nitrogen atmosphere (O_2 < 1 ppm) where the Cm(III) experiments were conducted. A stock solution of the long-lived curium isotope ^{248}Cm (half-life: 3.4 x 10^5 years) was used. This solution had the following composition: 97.3% ^{248}Cm, 2.6% ^{246}Cm, 0.04% ^{245}Cm, 0.02% ^{247}Cm, and 0.009% ^{244}Cm in 1.0 M $HClO_4$. The Cm(III) concentration in the reaction tubes was adjusted to 0.685 µM and 2.0 µM for site-selective TRLFS. The pH was measured using an InLab Solids combination pH puncture electrode (Mettler-Toledo, Giessen, Germany) calibrated with standard buffers. In all samples an initial increase in pH from 5.80 to 6.05 was measured after 24 h. After 7 d an average pH of 5.5±0.07 was reached. After the defined exposure times (0.5, 5, 24, 48, 72, 96, 120, 144, and 168 h), aliquots from the supernatants were separated from the samples. The supernatants were centrifuged (13,000 rpm, room temperature; centrifuge MiniSpin, Eppendorf, Hamburg, Germany) prior to determining Cm(III) concentration. The Cm(III) amount in supernatants was measured by liquid scintillation counting (LSC) with α/β discrimination using a Wallace 1414 LSC counter (PerkinElmer). From that the amount of bioassociated metal given in percent related to the initial amount of metal in the medium was calculated.

2.2. Statistical analyses

The statistical evaluation of selected experimental data (cell vitality, phenolic content, and Ca(II) + Mg(II) cell contents) of the Eu(III) experiments was performed by the two-tail student's t-Test using the implemented functions in the "Analysis ToolPak" of Microsoft Excel 2010. The p-value was used to discriminate between data groups showing significance ($p < 0.05$) and those that did not. One asterisk (p-

value less than 0.05) denotes statistical significance, while two asterisks indicates a very significant event (p-value less than 0.01). Also, p-values less than 0.1 can be interpreted as a strong tendency (++) and p-values less than 0.5 as a tendency (+)in the experimental data.

2.3. Time-resolved laser-induced fluorescence spectroscopy measurements (TRLFS)

2.3.1. Europium(III) – TRLFS with UV excitation

Eu(III) TRLFS studies were conducted as previously described (e.g., Moll et al., 2009; Moll et al., 2020a). Medium R_{red} (30 and 200 µM Eu(III)), supernatants, resuspended cells, and model solutions (30 µM Eu(III)) were measured in 1 cm quartz glass cuvettes (Hellma Analytics, Mühlheim, Germany). Cells were suspended in 0.154 M NaCl (pH = 5.8) at room temperature. Experimental details concerning the luminescence measurements and data evaluation can be found in the Supplementary Information section. The relative peak intensity ratio, $R_{E/M}$, which provides information about the ligand field of Eu(III) and the coordination environment, was determined by forming the ratio for the integral intensities I of the $^7F_2$ to $^7F_1$ band using equation SI3.

The number of coordinated water molecules was determined based on the work of Horrocks & Sudnick (Horrocks and Sudnick, 1979) and of Kimura and colleagues (Kimura et al., 1996), which is presented for europium in equation SI4.

2.3.2. Europium(III) – site selective TRLFS

The site-selective luminescence measurements, which used excitation wavelengths between 575 and 582 nm for direct excitation of Eu^{3+} ions from the ground $^7F_0$ state to the emitting $^5D_0$ state, were performed as previously described (Xiao et al., 2018). For lifetime measurements, the luminescence emissions were collected using a varied delay time from 20 to 35 µs with a total up to 75 steps. All samples were cooled to low temperature (T < 10 K) using a helium refrigerated cryostat (Cryophysics CCS 100, Cryophysics, Germany) to obtain the spectral resolution required to discriminate different crystal-field transition lines of Eu^{3+}. The solutions were placed in plastic cuvettes and shock-frozen with liquid nitrogen prior to conducting luminescence measurements.

2.3.3. Curium(III) - TRLFS with UV excitation

The experimental setup for the Cm(III) luminescence measurements are summarized in prior reports (e.g., Moll et al., 2009; Moll et al., 2020b). Supernatants and resuspended cells in 0.154 M NaCl were investigated in a 1 cm quartz glass cuvette under stirring at room temperature. Time-resolved measurements (300 lines/mm grating) were obtained by a dynamic step width to describe the species observed with long and short emission lifetimes (equation SI2). The decrease in luminescence was investigated over 35 to 50 time points, which resulted in 35 to 50 spectra. The evaluation of the luminescence data was performed as previously reported (Moll et al., 2020b). The number of coordinated water molecules around Cm(III) was determined based on the equation of Kimura and colleagues (Kimura et al., 1996), which is presented in Equation SI5.

2.3.4. Cm(III) site-selective TRLFS

The site-selective luminescence measurements using excitation wavelengths between 585 and 618 nm for direct excitation of Cm^{3+} ions from the ground $^{8}S_{7/2}$ state to the emitting $^{6}D_{7/2}$ state were performed as described in (Wolter et al., 2019). All other experimental details are similar as described for the Eu(III) site-selective TRLFS measurements.

3. Results and discussions

3.1. Bioassociation of Eu(III) and Cm(III) on Brassica napus suspension cells

The amount of Eu(III) bioassociated to *B. napus* cells was determined after 7 d of exposure (Fig. 1A, B). In addition, the effects of Eu(III) concentration and cell concentration on the homeostasis of intracellular Mg(II) and Ca(II), the most abundant ions in living systems, were explored. Based on resulting cell concentration data, we confirmed that *B. napus* suspension cells bioassociated a higher level of Eu(III) for the 40 g/L cell sample (0.30 and 3.2 µmol/$g_{fresh\ cells}$) in comparison to the 600 g/L cell sample (0.05 and 0.30 µmol/$g_{fresh\ cells}$). This finding indicates a cell concentration-dependent bioassociation capacity, which is indicative of biosorption.

The intracellular Mg(II) and Ca(II) content of the 600 g/L cell sample did not change significantly in the presence of Eu(III). In contrast, the intracellular Ca(II) content for the 40 g/L cells appeared to be slightly higher for those grown in the presence of Eu(III), as confirmed by statistical analysis (see below).

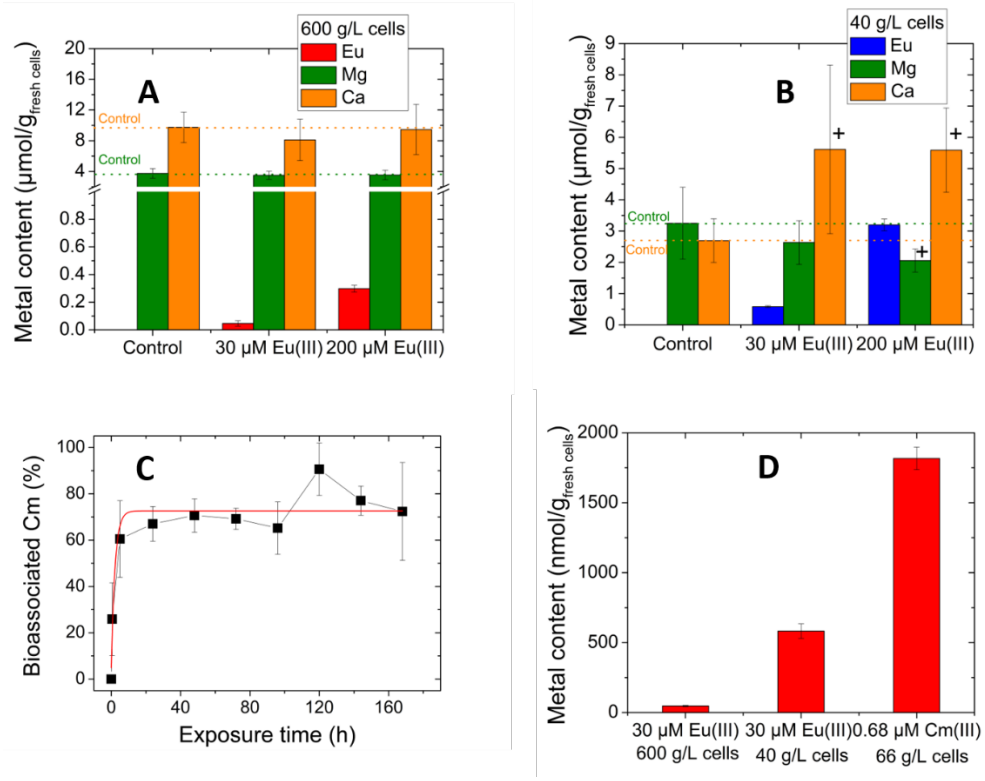

Fig. 1. Eu(III), 600 g/L cells (A) and 40 g/L cells (B), bioassociation by *B. napus* cells after an exposure time of 7 d and their effects on the homeostasis of intracellular Mg(II) and Ca(II). Data represent mean values ± standard error (SE) of five independent experiments for determining the bioassociated amount of Eu(III). Ca(II) and Mg(II) content was measured in three independent experiments. + ($p < 0.5$). (C) Time-dependent Cm(III) bioassociation by *B. napus* cells. Data represent mean values ± SE of three independent experiments covering different time spans between 0.5 and 168 h. (D) Comparison of the bioassociation of Eu(III) and Cm(III) by *B. napus* cells as a function of cell concentration.

The Mg(II) content appeared to be slightly lower for cells that were incubated in the presence of 200 µM Eu(III). Due to its ionic radius, Eu(III) is not only an analog for trivalent actinides (e.g. Cm(III) and Am(III)), but can also serve as an analog for Ca(II) (Drobot et al., 2019; Schmidt et al., 2008; Holliday et al., 2012). To date, research indicates that substituting Eu(III) for Ca(II)/Mg(II) does not appear to impact the normal physiological functions of plant tissues; in contrast, the phytotoxic effects of Eu(III) are unknown (Fellows et al., 2003; Martinez-Gomez and Skovran, 2016). What is known is that Eu(III) can

directly enter plant cells through endocytosis (Wang et al., 2014) or via the lanthanide-induced permeability of the plasma membrane (Yamasaki et al., 2013). As a consequence, Eu^{3+} competes with Ca^{2+} for protein binding sites. Our observation of a slightly increased Ca(II) uptake, with only small changes in the Mg(II) content of the cells for samples Eu03040-C and Eu20040-C, upholds the earlier findings of Vanhoudt et al. (2010), who reported enhanced Ca(II) uptake and almost unchanged Mg(II) concentration in the roots of *Arabidopsis thaliana* seedlings in the presence of U and Cd (Vanhoudt et al., 2010). The observed increase in Ca(II) uptake likely corresponds to the cells' defense mechanism against Eu(III) toxicity, which is supported by our results for cell growth, cell vitality, and the phenolic content of the cells in the presence of Eu(III). Specifically, we recorded inhibited cell growth paired with a significant decrease in cell vitality and phenolic content, especially for the highest Eu(III)-to-cell ratio, which reflects the phytotoxic effect of Eu(III) under these experimental conditions. These results are discussed in greater detail in the supporting information (Fig. S1, Fig. S2, and Fig. S3).

Our previous work with *B. napus* callus cells exposed to 30 and 200 µM Eu(III) showed that 0.03 and 0.63 $\mu mol/g_{fresh\ cells}$ of Eu(III) were associated to the cells, respectively. In contrast, suspension cells accumulated significantly higher (5 – 10x) amounts of Eu(III), 0.30 and 3.2 $\mu mol/g_{fresh\ cells}$, respectively. These findings confirmed that cells suspended in medium R_{red} supplemented with Eu(III) evidence a high binding affinity for Eu(III). We attribute this result to the fact that the Eu(III)-containing medium bathed the suspension cells, thereby providing a larger cell surface available for Eu(III) binding compared to callus cells grown on a solid medium. We also observed a rapid biosorption process for Cm(III) (cf. Fig. 1C); specifically, after only 5 h of incubation the bioassociation level approached an equilibrium of 1.82 $\mu mol/g_{fresh\ cells}$ biosorbed Cm(III) on *B. napus* cells. Moreover, vitality-related experiments involving our control cells in the glovebox showed a decrease in cell vitality to only ~4% after incubation for 72 h. The inert atmosphere in the glove box, the lack of nutrients, and the presence of the α-emitter Cm(III) represent notable factors for the observed decrease in cell vitality. Consequently, our findings indicate that near-metabolically inactive cells also associated Cm(III), but that significantly higher amounts are associated compared with active cells for Eu(III) (cf. Fig. 1D; Fig. S2).

3.2. Cm(III) and Eu(III) as molecular probes for speciation analyses

3.2.1. Results of Cm(III) - TRLFS

For the first time, we report Cm(III) luminescence data in the presence of plant cells (cf. Fig. 2) with subsequent Cm(III) speciation analyses (cf. Fig. 3).

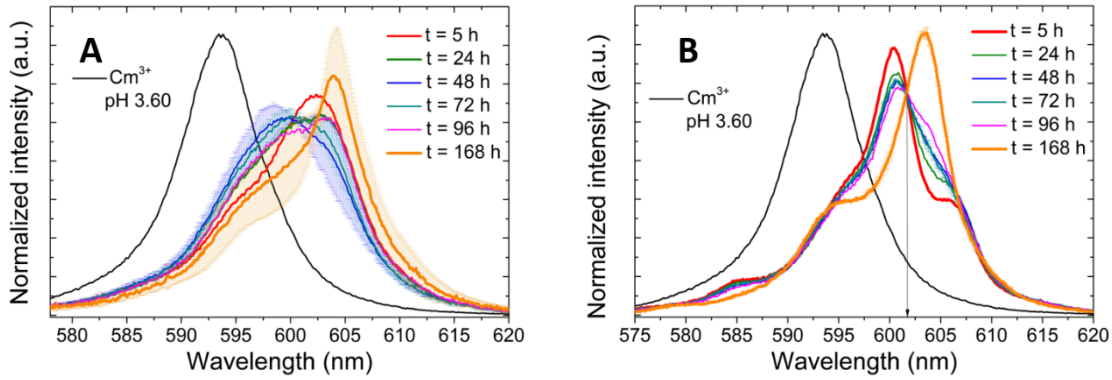

Fig. 2. Cm(III) luminescence spectra in the presence of *B. napus* cells (samples Cm000766-S and –C). A) Supernatants after separation of the cells by centrifugation, pH = 5.70. B) Cm(III)-loaded cells, pH = 5.50.

Note that a strong red shift in the emission maximum to 602.4 nm was observed in the supernatant after a short exposure time of just 5 h (Fig. 2A). We also recorded an unsystematic behavior of the emission maximum: first to 602.4 nm then back to 599.7 nm and finally to 604.2 nm after 168 h. For all supernatants, a bi-exponential luminescence decay was measured: 108 ± 9 µs (N_{H2O} = 5.1) and 260 ± 29 µs (N_{H2O} = 1.6) (cf. Table 2). These results indicate the occurrence of at least two Cm(III)-supernatant species. Again, no systematic lifetime trends as a function of exposure time were observed. Nonetheless, both the red shift of the peak maximum and the longer lifetimes (both relative to the Cm aquo ion), indicate a change in the coordination of Cm. It could be that stressed or lysed *B. napus* cells liberate agents to complex Cm(III) very quickly in the solution surrounding the cells. Hence, the rapid biosorption process is accompanied by rapid Cm(III) complexation with substances released from the cells. Solid phase extractions of the supernatant with subsequent HPLC analyses demonstrated the presence of metabolites (such as low-molecular phenolic compounds) and/or cell components.

TRLFS measurements of the cells reveal that the rapid Cm(III) biosorption process to the cells induced a red shift in the emission spectra from 593.7 to 600.4 nm after 5 h of exposure (Fig. 2 B). The intensity at ~600 nm initially decreased, but then increased at 603.5 nm as a function of exposure time. Finally, the emission maximum at 603.5 nm was observed to dominate the sum spectrum. The spectra of all Cm(III)-loaded cells as a function of exposure time featured one isosbestic point at 601.7 nm. The isosbestic point indicates a simple time-dependent chemical reaction characterized by a defined stoichiometric relationship

between the reactants. At the observed point in this study, the normalized luminescence intensities of the reactants were noted to be equal. The number of points, here one, is a measure for the number of reaction steps (Schläfer and Kling, 1956).

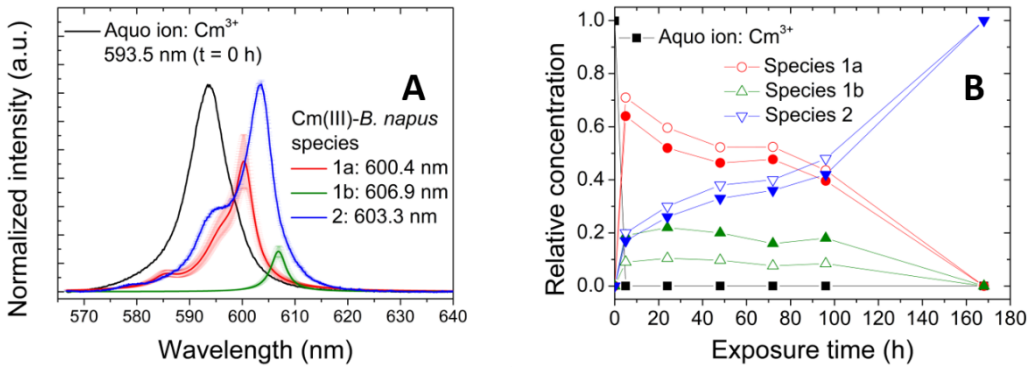

Fig. 3. Results of the deconvolution of the sum spectra of Cm(III)-loaded *B. napus* cells (resuspended cell data). A) Extracted single component spectra. B) Spectroscopic Cm(III) species distribution (open symbols: no FI used, filled symbols: FI used, FI: relative fluorescence intensity factor).

For the Cm(III)-loaded cells, a bi-exponential luminescence decay was observed within the investigated time span. On the basis of TRLFS data, one Cm(III)-species featured a lifetime of 133 ± 17 µs (N_{H2O} = 4.0), whereas the second Cm(III)-species displayed a lifetime of 366 ± 28 µs (N_{H2O} = 0.9) (Table 2).

In an initial attempt to deconvolute the Cm spectra, we applied the ITFA algorithm. The resulting spectra calculations of resuspended cells for Cm(III)−*B. napus* species 1 yielded a spectrum depicting an emission maximum at 600.5 nm and a shoulder at 606.7 nm (cf. Fig. S4, S5), which is quite unusual for Cm(III) single-component spectra. In general, Cm(III) species are characterized by a single red-shifted emission maximum and, if resolved, blue-shifted hot bands in front of the emission maximum (Edelstein et al., 2006).

Table 2: Luminescence maxima and lifetimes of Cm(III) species in the *B. napus* system and Cm(III) species with relevant references (pH range: ca. 4 to 9).

Species	Emission (nm)	Lifetime (µs)	$N_{H2O} \pm 0.5$ H_2O	Comments	Reference
Cm^{3+} (aq)	593.6	68.5 ± 1.5	8.6		This work
Cm^{3+}-*B. napus* species					
Cell species 1	600.5 [b]	133 ± 17	4.0	Bi-exponential	This work
Cell species 2	603.4	366 ± 28	0.9		
Supernatant species 1	603.9	108 ± 9	5.1	Bi-exponential	This work
Supernatant species 2	599.4	260 ± 29	1.6		
Microbes					
Cm^{3+}– *Sporomusa* sp.: R–O–PO_3H–Cm^{2+}	599.8	252 ± 46	1.7	Bi-exponential	Moll et al., 2014
Cm^{3+}– *Sporomusa* sp.: R–COO–Cm^{2+}	601.6	108 ± 15	5.2		
Cm^{3+}-yeast isolate *R. mucilaginosa* BII-R8 species 1	599.6	240 ± 50	1.8	Bi-exponential	Lopez-Fernandez et al., 2019
Cm^{3+}-yeast isolate *R. mucilaginosa* BII-R8 species 2	601.5	123 ± 11	4.4		
Cm^{3+}–*Pseudomonas fluorescens*: R–O–PO_3H–Cm^{2+}	599.6	390 ± 78	0.8	Bi-exponential	Moll et al., 2013
Cm^{3+}–*Pseudomonas fluorescens*: R–COO–Cm^{2+}	601.9	121 ± 10	4.5		
Cm^{3+}–*Desulfovibrio aespoeensis* complex	600.1	162 ± 5	3.1	Mono-exponential	Moll et al., 2004
Cm^{3+}–*Paenibacillus* sp. complex: R–O–PO_3H–Cm^{2+}	598.8	477 ± 73	0.5	Mono-exponential	Lütke, 2013
Biopolymers with phosphate / carboxyl / amino groups					
LPS (*Pseudomonas aeruginosa*): R–O–PO_3H–Cm^{2+}	599.9	150	3.5	Bi-exponential	Moll et al., 2009
LPS (*Pseudomonas aeruginosa*): R–COO–Cm^{2+}	602.3	100 214	5.6 2.2	Mono-exponential	
Biopolymers with carboxyl / amino groups					
PG (*Bacillus subtilis*): R–COO–Cm^{2+}	602.0	230	1.9	Mono-exponential	Moll et al., 2009
Proteins: carboxyl / amino / hydroxyl groups					
Cm(III)-transferrin species I	599.8	~ 100	~ 5		Bauer and Panak, 2015
α-amylase: $Cm(Amy\text{-}COO)^{2+}$	~ 597	120 ± 10	4.5	Bi-exponential	Barkleit et al., 2016
α-amylase: $Cm(Amy\text{-}COO)_3$	~ 603	240 ± 40	1.8		
Calmodulin: Cm-CaM species 2 [a]	605.2	204 ± 22	2.4	Mono-exponential	Drobot et al., 2019
Native S-layer protein from *Lysinibacillus sphaericus* JG-A12[a]	602.2 607.6	142 ± 29 334 ± 33	3.7 1.1	Bi-exponential	Moll et al., 2020b

N: number of coordinated water molecules. LPS: lipopolysaccharide. PG: peptidoglycan. [a] Influence of phosphate groups possible. [b] Main emission band.

Our series of ITFA calculations showed that this shoulder could not be compensated by species 2. Hence, a manual deconvolution of the sum spectra was performed using the spectrum at 168 h as a pure component spectrum for species 2. This approach is supported by the fact that measurements of cell suspensions after 120 and 144 h of exposure evidenced the same spectrum. The factor-weighted spectrum of species 2 was subtracted from the sum spectra at 5, 24, 48, 72, and 96 h; a sufficient separation of both emission maxima at 600.5 and 606.7 nm was the criterion for the factor. Hence, the resulting spectrum is comprised of species 1a and 1b. Using the peak fit function (Lorentz) of Origin, we then separated species 1a and 1b (see Figure 3 A); the corresponding species distribution is depicted in Figure 3 B (open symbols). Relative fluorescence intensity factors (FI) for each individual species (i) are required to obtain a relative speciation of the resulting species. The procedure describing the calculation of the current FI's is summarized in the Supplementary information section. The species distribution of Cm(III) in the presence of *B. napus* cells after FI correction can be seen in Figure 3 B (filled symbols). Importantly, the influence of species 1b would be significantly underestimated without an FI correction. We observed the very rapid formation of Cm(III)−*B. napus* species 1 with an equilibrium between species 1a and 1b. With increasing exposure time, a decrease of Cm(III)−*B. napus* species 1 and an increase of Cm(III)−*B. napus* species 2 was observed.

Based on the results provided in Table 2, one can derive estimates concerning the nature of the binding sites afforded by the cells and the metabolites/cell components in the supernatants for Cm(III) coordination. Cm(III) coordinated to phosphate groups of microbial origin is characterized by an emission maximum at ~600 nm, with two coordinated H_2O molecules on average. In contrast, Cm(III) bound to carboxyl groups of microbial origin and in proteins demonstrates a more red-shifted emission maximum at 602.0 ± 0.3 nm, with four coordinated H_2O molecules. For carboxyl groups in proteins, the spectral range of maxima, ± 4 nm, is much broader. This expanded emission maxima range could indicate the greater influence of the respective binding pocket of the individual protein. The emission maxima for species 3 (in the supernatant) and 1a (on the cells) are located within the range of microbial phosphate groups. Conversely, the analogous data for species 1 (in the supernatant) and 2 (on the cells) could indicate an interaction with carboxyl groups. Finally, the most red-shifted emission maxima for species 2 (supernatant) and 1b (cells) may indicate Cm(III) binding to proteins.

We then utilized site-selective TRLFS for a comprehensive characterization of Cm(III)-*B. napus* species 2, which dominated over long exposure times. For the first time, this study demonstrates the application of site-selective TRLFS to a biological system. The excitation spectrum of Cm(III)-loaded *B. napus* cells

yielded two broad bands at ~594 and ~602 nm (Fig. 4). Note that the shape of the spectrum is similar to the corresponding emission spectrum after excitation at 396.6 nm (Fig. 2B). We detected a similar emission spectrum nearly independent of the excitation wavelength. The most significant observed difference was the narrowing of the line that occurred upon excitation in the range of the second band ~602 nm (Fig. 4). These results suggest the occurrence of one Cm(III) species surrounded with a continuous distribution of slightly different Cm(III) coordination environments. Hence, Cm(III)-*B. napus* species 2 is characterized by a main emission band at 602 nm and a hot band of this transition at 594 nm. Independent of the excitation wavelength, a bi-exponential luminescence decay was always measured with lifetimes of 145 ± 10 and 366 ± 15 µs (Fig. S7). Both lifetime results are in excellent agreement with the findings from room temperature TRLFS after UV excitation (Table 2). This bi-exponential luminescence decay and the slightly red-shifted emission spectrum after excitation at 594.8 nm at a delay of 600 µs compared with 1 µs (Fig. S8), suggested the simultaneous excitation of a minor Cm(III) species.

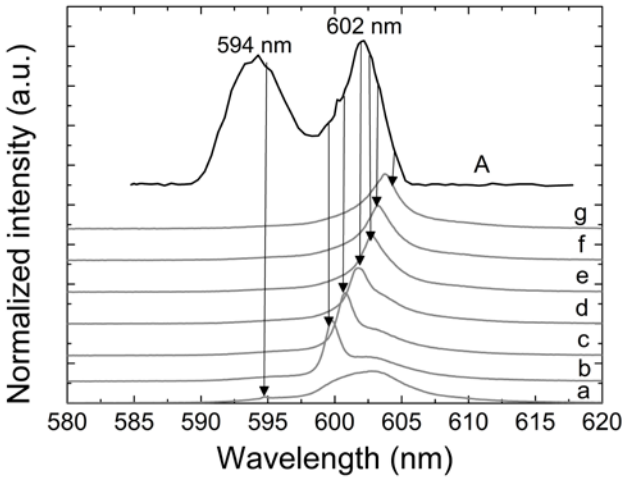

Fig. 4. Excitation spectra (A, top black line) of Cm(III)-loaded *B. napus* cells (Cm00269-C, exposure time: 168 h) and recorded emission spectra (a-g, gray lines) after excitation at different wavelength: (a) 594.8 nm, (b) 599.8 nm, (c) 600.8 nm, (d) 601.8 nm, (e) 602.8 nm, (f) 603.3 nm, and (g) 603.8 nm.

In conclusion, at an exposure time of 168 h, the Cm(III) speciation on *B. napus* cells was found to be dominated by Cm(III)-*B. napus* species 2 with a continuous distribution of slightly different Cm(III) environments.

3.2.2. Results of Eu(III) – TRLFS with UV excitation

Following an exposure time of 7 d, we obtained the luminescence spectra for Eu(III), both bioassociated by *B. napus* cells and in the supernatant, as a function of the initial Eu(III) concentration and cell concentration, which are depicted in Figure S10 and Table SI3. The results obtained with samples Eu03040 and Eu20040 are summarized in the Supporting information section (Fig. S11, Table SI4). The interaction of Eu(III) with *B. napus* cells can be directly observed in changes of the ratio between the $^7F_1$ (~591 nm) and the hypersensitive $^7F_2$ peak at about 616 nm ($R_{E/M}$), the occurrence of the symmetry-forbidden $^7F_0$ peak as well as in the luminescence lifetimes (Fig. S10, Table SI3, Table SI4 Figs. S11, S12). Compared to the Eu(III) in the medium and the supernatants, the spectrum of Eu(III) bioassociated to the plant cells is characterized by both changes in the shape of the transitions (cf. Fig. S10A and B, Fig. S11) and lifetime (cf. Fig. S12, Tables SI3 and SI4), hence, differences in the Eu(III) speciation can be expected.

Moreover, the luminescence spectra of the supernatants are characterized by enhanced $R_{E/M}$ values of 2.2 ± 0.3, equation (SI3), in comparison to the Eu(III) aquo ion and Eu(III) in the medium (cf. Table SI3, Table SI4).. We also detected bi-exponential luminescence decay in our plant cell samples and supernatants, indicating the occurrence of at least two different Eu(III) coordination environments for each.

In general, the Eu(III) species in the supernatants and on the cells evidence longer lifetimes compared to the medium. The short lifetime demonstrated a reduced dependence on the initial Eu(III) concentration. Supernatants displayed lifetimes between 115 and 138 µs, corresponding to nine and seven coordinated water molecules, respectively. The first Eu(III) complex on *B. napus* suspension cells showed lifetimes between 145 and 158 µs, corresponding to seven and six coordinated water molecules, respectively. For the long lifetime of the second Eu(III) complex in the supernatants, we noted a strong correlation with initial Eu(III) concentration. At the initial concentration of 30 µM Eu(III), a lifetime of 450 µs ($N_{2,\,H2O}$ = 2.0) was measured, whereas the lifetime at 200 µM Eu(III) was determined to be 270 µs ($N_{2,\,H2O}$ = 3.5). The longest lifetime was detected for the second Eu(III) complex on the suspension cells with 600 µs ($N_{2,\,H2O}$ = 1.2). This significant change in the hydration sphere of Eu(III) indicates the bioassociation of Eu(III) with *B. napus* cells. These lifetime results for both Eu(III) species are comparable to our previous study, suggesting that similar Eu(III) species are formed on callus and suspension cells of *B. napus*.

To explore the nature of the Eu(III) binding sites on *B. napus* cells, selected model compounds with organic phosphate and carboxyl groups were investigated. The luminescence spectra of all model compounds and their structures are summarized in the Supplementary information section (cf. Fig. S13, S14). Our resulting data confirmed that the Eu(III) cell spectrum was very similar to the Eu(III) spectrum

with phytic acid. Based on carboxylic reference data, oxalic, citric, and malonic acid were most similar to the Eu(III) spectrum. Hence, we suggest the involvement of organic phosphate and carboxyl groups in Eu(III) binding, which is in good agreement with our observations for the Cm(III) system.

Based on experimentally obtained lifetime measurement data, Ozaki et al. confirmed a relationship between $R_{E/M}$, the strength of the ligand field, and the geometrical structure around Eu(III) (Ozaki et al., 2002). This empirical approach, which relies on the construction of coordination environment (CE) diagrams, was found to be effective for characterizing the coordination environment of both hydrated and complexed Eu(III) in a variety of systems (e.g. Moll et al., 2014; Sachs et al., 2015). More information concerning the CE diagram can be found in the Supplementary information section. The data points corresponding to the medium, supernatant, and cells on our $R_{E/M}$-ΔN_{H2O} plot are scattered in the upper-left area of Figure S15, which is characteristic for predominant inner-sphere coordination. Based on the position of our data points, we can postulate the following sequence of decreasing degrees of binding strength: cells and supernatants at 30 µM Eu(III) > cells and supernatants at 200 µM Eu(III) >> medium. The Eu(III) coordination environment of Eu(III)-loaded cells and supernatants at 30 µM Eu(III) were similar to those found for *B. napus* callus cells grown on solid medium with 200 µM Eu(III), although they exhibited strongly different Eu(III) loadings (i.e., 0.63 µmol/$g_{\text{fresh cells}}$ and 3.2 µmol/$g_{\text{fresh cells}}$ for 40 g/L cells, respectively). Moreover, the Eu(III) coordination environment in the Eu-loaded cells and supernatants at 200 µM displayed similarities with (a) Eu(III) bound to the bacterial phosphate groups of the cell envelope of *Sporomusa* sp. (Moll et al., 2014), (b) organic phosphate and carboxyl groups of *Shewanella putrefaciens* (Ozaki et al., 2005), (c) bacterial lipopolysaccharide (Moll et al., 2009; Bader et al., 2019), (d) Eu(III) complexed by the strong chelate-ligand EDTA, and (e) Eu(III) complexed by carboxyl groups of salicylic acid (Barkleit et al., 2013).

For the medium R_{red}, the Eu(III) coordination environment was similar to that of Eu(III) complexed by carboxyl groups of citric and oxalic acid.

Carboxyl and phosphate groups have been identified as major binding partners for Eu(III) on the cell wall of, for example, gram-negative bacteria. One molecule of these groups can provide at most bidentate coordination with Eu(III). From measured ΔN_{H2O}-values ranging between 3 and 6, Ozaki et al. concluded an inner-spherical Eu(III) coordination with more than one involved functional group (Ozaki et al., 2005). In our study, we determined ΔN_{H2O}-values greater than 6 for cells and supernatants; additionally, we also confirmed carboxyl and phosphate groups to be significant functional groups involved in Eu(III) binding

on plant cells. Hence, an inner-spherical Eu(III) coordination involving more than one functional group was found to be dominant in our samples. The involvement of carboxyl groups in Eu(III) binding on *B. napus* cells is also in agreement with earlier results reported by Drake et al. based on their Eu(III) studies with native *Datura innoxia* cell wall fragments and Biorex resin (Table SI3) (Drake et al., 1997). Specifically, Drake and coworkers identified four unique binding sites on cell wall fragments, whereas the higher affinity sites involve carboxylate groups for Eu(III) uptake. It must be noted, however, that we cannot as yet discount the potential contribution of other functionalities (e.g., phosphate groups). As we previously reported, *B. napus* suspension cells provide multiple-binding environments for Eu(III), although some binding sites do exhibit relatively poor luminescent properties.

3.2.3. Site-selective TRLFS – Excitation of the non-degenerate $^5D_0 \rightarrow {}^7F_0$ transition

After analyzing the cells, supernatant, and medium, excitation spectra were assessed for the Eu(III)-*B. napus* system. As shown in Figure 5, the spectra were found to be characterized by rather broad excitation bands, which indicate poorly defined ligand fields in the biological matrix, e.g. as a continuum of similar but distinct environments. We also observed similar behavior for the excitation spectra of Eu(III)-containing biogenic $CaCO_3$ produced by *Sporosarcina pasteurii* (Johnstone et al., 2016). The spectral position of the $^5D_0 \rightarrow {}^7F_0$ transition and $R_{E/M}$ values of Eu(III) *B. napus* samples are provided in Table SI6.

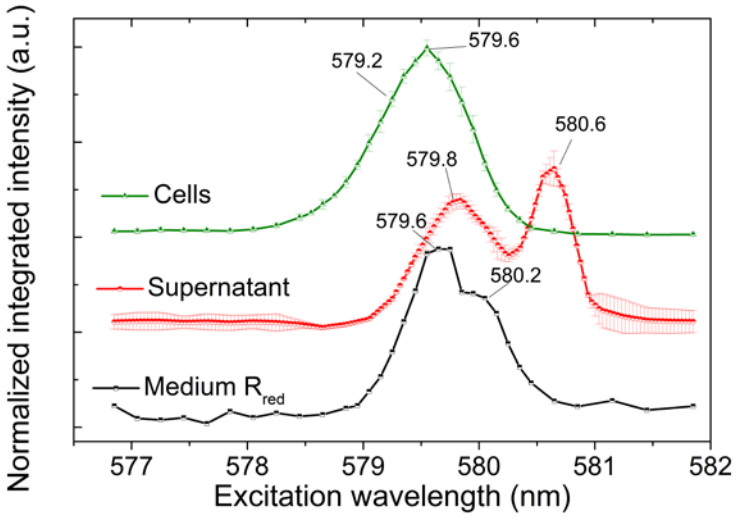

Fig. 5. $^7F_0 \rightarrow {}^5D_0$ excitation spectra of the Eu(III) in *B. napus* samples (200 µM Eu(III), 40 g/L cells, T: 10 K).

Our resulting excitation spectra are characterized by red-shifted maxima compared to the excitation maximum for $Eu(H_2O)_9^{3+}$ at 578.8 nm (Carlos et al., 2005). For the spectrum of Eu(III) medium R_{red}, one absorption maximum was observed at 579.6 nm, together with a shoulder at 580.2 nm (Fig. 5). Luminescence lifetime data captured after excitation close to the maximum (at 579.8 nm) was characterized by mono-exponential behavior with a value of 638 ± 29 µs (Table SI7), which is consistent with one coordinating H_2O molecule. For the emission spectrum, broad $^7F_1$ and $^7F_2$ transitions were observed (Fig. S16). When exciting in the shoulder region of the spectrum at 580.2 nm, a shorter lifetime (437 ± 34 µs) was determined (Table SI7). This lifetime is consistent with two coordinated H_2O molecules. In the emission spectra of both species, a 3-fold splitting of the $^5D_0 \rightarrow {}^7F_1$ and a 4-fold splitting of the $^5D_0 \rightarrow {}^7F_2$ transition were observed, though both were poorly resolved.

With respect to analogous findings for the supernatants, two different excitation species were also observed (Fig. 5). The first species features an excitation band at 579.8 nm, with a luminescence lifetime of 431 ± 15 µs, corresponding to two coordinated H_2O molecules. The emission spectrum showed a 3-fold splitting of the $^7F_1$ transition together with an unresolved splitting pattern for the $^7F_2$ transition; its lifetime is identical to that of the second Eu(III) species in the medium, and the emission spectra are also similar. Thus, it is possible that this species is the same in both the medium and supernatant, which would suggest binding to a constituent of the medium rather than a metabolite of the cells, which could only be observed in the supernatant. The second supernatant species showed a strongly red-shifted maximum at 580.6 nm (Fig. 5, Table SI6). This species could be an analog to the equally strongly red-shifted Cm(III) species 2 observed in the supernatants (cf. Fig. S4). Note that luminescence decay results were mono-exponential with $\tau = 984 \pm 34$ µs, which corresponds to 0.5 coordinated H_2O molecules (Table SI7). These observations indicate strong changes in the coordination sphere of Eu(III). The emission spectrum displayed a 3-fold splitting of the $^7F_1$ band combined with a 3-fold splitting of the $^7F_2$ band.

The excitation spectrum of the Eu(III)-loaded cells showed a broad band at 579.6 nm with indications for a shoulder at 579.2 nm. Based on bi-exponential decay data after an excitation at 579.6 nm with lifetimes of 147 ± 28 µs (N_{H2O} = 6.7) and 694 ± 24 µs (N_{H2O} = 0.9), we can conclude a simultaneous excitation of multiple species. These lifetime results demonstrate that different Eu(III) species are present compared with those in the medium and the supernatants. Again a 3-fold splitting of the $^7F_1$ band in the emission spectrum (Fig. S16) indicates the formation of low-symmetry Eu(III) species (Binnemans, 2015), as also observed for the other species in our samples.

For a more comprehensive description of the excitation spectrum of the Eu(III)-loaded biomass, suitable references are provided (Fig. S17, Fig. S18). The best fit was achieved by combining the spectra of 61% malonic acid, 33% phosphoenolpyruvate, and small amounts of citric and oxalic acid, indicating that ~67% of Eu(III) is bound to carboxyl and ~33% to phosphate groups of *B. napus* cells. Hence, results from this study confirm conclusions from our earlier work demonstrating that organic carboxyl and phosphate groups of the cells are involved in M(III) binding.

4. Conclusions

For this study we compared the interaction of *B. napus* suspension cells (40, 66, and 600 g/L) with two trivalent f-elements, Eu(III) and Cm(III), in a broad concentration range from 0.67 µM to 200 µM, with results indicating that bioassociation depends on both M(III) and cell concentration. Specifically, we determined a strong increase in the amount of bioassociated Eu(III) from 0.30 to 3.2 µmol/$g_{\text{fresh cells}}$ at 30 and 200 µM Eu(III), respectively, at 40 g/L cells. Our experimental findings support a strong inhibition of cell growth in the presence of 200 µM Eu(III), and a decrease in both cell vitality and the production of phenolic compounds, all of which can be attributed to the toxic effects of Eu(III). We also conclude that bioassociated Eu(III) has a tendency to influence the homeostasis of intracellular Mg(II) and Ca(II), as evidenced by the fact that the cells responded with higher Ca(II) contents and lower Mg(II) contents at 40 g/L cells. For Cm(III), a dominant biosorption mechanism was discovered whereby near-metabolically inactive cells can accumulate large amounts of Cm(III) (i.e., 1.82 µmol/$g_{\text{fresh cells}}$).

Spectroscopically, we observed strong inner-sphere Eu(III) complexes formed in both the supernatants and on the cells for cell-bound Eu(III). Resulting data associated with the Eu(III) site-selective luminescence spectra of cells, obtained by linear regression with spectra of reference compounds, confirmed the contribution of both carboxyl and organic phosphate groups in Eu(III) binding, with a preference for the former.

For Cm(III), we also observed two different main species in both the supernatants and on the cells. Based on the emission maxima and the lifetime results obtained for Cm(III)-*B. napus* cell species, we suggest the involvement of protein-based carboxyl groups in Cm(III) coordination. However, the contribution of organic phosphate groups is also possible. To conclude, *B. napus* suspension cells provide multiple carboxylic and phosphatic environments for binding Eu(III) and Cm(III).

The integrative approach of our study, which incorporated biological, biochemical, and multiple spectroscopic methods, further enhanced our understanding of the interactions of trivalent f-elements with plant cells at the molecular level. At this point in time, however, we need additional knowledge to fully elucidate the macroscopic process.

CRediT authorship contribution statement

Henry Moll: Conceptualization, Sample preparation, Data acquisition, Data analyses, Writing; Moritz Schmidt: Data acquisition, Writing; Susanne Sachs: Sample preparation, Data acquisition, Data analyses, Writing.

Declaration of Competing Interests

The authors declare that they have no known competing financial interests or personal relationships that could have appeared to influence the work reported in this paper.

Acknowledgements

The authors are indebted to the U.S. Department of Energy, Office of Basic Energy Sciences, for the use of ^{248}Cm via the transplutonium element production facilities at Oak Ridge National Laboratory; ^{248}Cm was made available as part of collaboration between HZDR and the Lawrence Berkeley National Laboratory (LBNL). We thank Jana Seibt, Sylvia Heller, Jenny Jessat for their invaluable help in carrying out our experimental assays; we also acknowledge the contributions of Sabrina Beutner and Birke Pfützner for assistance with ICP-MS measurements; and we are thankful to Frank Bok for thermodynamic Eu(III) speciation calculations. We acknowledge the help of Nina Huittinen and Manuel Eibl in performing the site-selective TRLFS investigations. We also thank Laurie S. Good for proofreading of the article. This work was partly funded by the German Federal Ministry of Education and Research under contract number 02NUK051B.

References

Adriano, D.C., McLeod, K.W., Ciravolo T.G., 1981. Curium uptake by crops from naturally-weathered contaminated soil. Health Phys. 41, 69-75. https://doi.org/10.1097/00004032-198107000-00007.

Ansoborlo, E., Prat, O., Moisy, P., Den Auwer, C., Guilbaud, P., Carrière, M., Gouget, B., Duffield, J.R., Doizi, D., Vercouter, T., Moulin, C., Moulin, V., 2006. Actinide speciation in relation to biological processes. Biochimie 88, 1605–1618. https://doi.org/10.1016/j.biochi.2006.06.011.

Bader, M., Moll, H., Steudtner, R., Lösch, H., Drobot, B., Stumpf, T., Cherkouk, A., 2019. Association of Eu(III) and Cm(III) onto an extremely halophilic archaeon. Environ. Sci. Pollut. Res. 26, 9352-9364. https://doi.org/10.1007/s11356-019-04165-7.

Barkleit, A., Acker, M., Bernhard, G., 2013. Europium(III) complexation with salicylic acid at elevated temperatures. Inorg. Chim. Acta 394, 535–541. https://doi.org/10.1016/j.ica.2012.09.014.

Barkleit, A., Heller, A., Ikeda-Ohno, A., Bernhard, G., 2016. Interaction of europium and curium with alpha-amylase. Dalton Trans. 45, 8724–8733. https://doi.org/10.1039/C5DT04790K.

Bauer, N., Panak, P.J., 2015. Influence of carbonate on the complexation of Cm(III) with human serum transferrin studied by time-resolved laser fluorescence spectroscopy. New J. Chem. 39, 1375–1381. https://doi.org/10.1039/C4NJ01877J.

Binnemans, K., 2015. Interpretation of europium(III) spectra. Coord. Chem. Rev. 295, 1-45. https://doi.org/10.1016/j.ccr.2015.02.015.

Bondar'kov, M.D., Ivanov, Yu.A., Zheltonozhskii, V.A., Zheltonozhskaya, M.V., 2006. Determination of the plutonium content in samples from a 30-km zone around the Chernobyl nuclear power plant. At. Energy 100, 144-148. https://doi.org/10.1007/s10512-006-0061-0.

Cao, D., Yang, X., Geng, G., Wan, X., Ma, R., Thang, Q., Liang, Y., 2018. Absorption and subcellular distribution of cadmium in tea plant (*Camellia sinensis* cv. "Shuchazao"). Environ. Sci. Pollut. Res. 25, 15357-15367. https://doi.org/10.1007/s11356-018-1671-5.

Carlos, L.D., Malta, O.L., Albuquerque, R.Q., 2005. A covalent fraction model for lanthanide compounds. Chem. Phys. Lett. 415, 238–242. https://doi.org/10.1016/j.cplett.2005.09.001.

Drake, L.R., Hensman, C.E., Lin, S., Rayson, G.D., Jackson, P.J., 1997. Characterization of metal ion binding sites on *Datura innoxia* by using lanthanide ion probe spectroscopy. Appl. Spectrosc. 51, 1476-1483. https://doi.org/10.1366%2F0003702971939253.

Drobot, B., Schmidt, M., Mochizuki, Y., Abe, T., Okuwaki, K., Brulfert, F., Falke, S., Samsonov, S.A., Komeiji, Y., Betzel, C., Stumpf, T., Raff, J., Tsushima, S., 2019. Cm^{3+}/Eu^{3+} induced structural, mechanistic and functional implications for calmodulin. Phys. Chem. Chem. Phys. 21/, 21213–21222. https://doi.org/10.1039/c9cp03750k.

Edelstein, N.M., Klenze, R., Fanghänel, T., Hubert, S., 2006. Optical properties of Cm(III) in crystals and solutions and their application to Cm(III) speciation. Coord. Chem. Rev. 250, 948-973. https://doi.org/10.1016/j.ccr.2006.02.004.

Fellows, R.J., Wang, Z., Ainsworth, C.C., 2003. Europium uptake and partitioning in Oat (*Avena sative*) roots as studied by laser-induced fluorescence spectroscopy and confocal microscopy profiling technique. Environ. Sci. Technol. 37, 5247-5253. https://doi.org/10.1021/es0343609.

Görller-Walrand, C., Binnemans, K., 1996. Handbook on the Physics and Chemistry of Rare Earths Volume 23, Chapter 155 Rationalization of crystal-field parametrization. Series Editors: Gschneidner, K.A. and Eyring, L., Pages 121-283.

Holliday, K., Handley-Sidhu, S., Dardenne, K., Renshaw, J., Macaski, L., Walther, C., Stumpf, T., 2012. A new incorporation mechnaism for trivalent actinides into bioapatite: A TRLFS and EXFAS study. Langmuir, 3845-3851. https://doi.org/10.1021/la300014a.

Horrocks, D.W. Jr, Sudnick, D.R., 1979. Lanthanide ion probes of structure in biology - laser-induced luminescence decay constants a direct measure of the number of metal-coordinated water-molecules. J. Am. Chem. Soc. 101, 334-340. https://doi.org/10.1021/ja00496a010.

Huang, G., Jin, Y., Zheng, J., Kang, W., Hu, H., Liu, Y., Zou, T., 2017a. Accumulation and distribution of copper in castor bean (*Ricinus communis L.*) callus cultures: in vitro. Plant Cell Tiss. Organ. Cult. 128, 177-186. https://doi.org/10.1007/s11240-016-1097-z.

Huang, D., Gong, X., Liu, Y., Zeng, G., Lai, C., Bashir, H., Thou, L., Wang, D., Xu, P., Cheng, M., Wan, J., 2017b. Effects of calcium at toxic concentrations of cadmium in plants. Planta 245, 863-873. https://doi.org/10.1007/s00425-017-2664-1.

Jessat, J., Sachs, S., Moll, H., Steudtner, R., Bok, F., Stumpf, T., 2021. Bioassociation of U(VI) and Eu(III) by *Brassica napus* suspension cell cultures – a spectroscopic investigation. Environ. Sci. Technol., under review.

Johnstone, E.V., Hofmann, S., Cherkouk, A., Schmidt, M., 2016. Study of the interaction of Eu^{3+} with microbiologically induced calcium carbonate precipitates using TRLFS. Environ. Sci. Technol. 50, 12411−12420. https://doi.org/10.1021/acs.est.6b03434.

Kimura, T., Choppin, G.R., Kato, Y., Yoshida, Z., 1996. Determination of the hydration number of Cm(III) in various aqueous solutions. Radiochim. Acta 72, 61-64. https://doi.org/10.1524/ract.1996.72.2.61.

Küpper, H., Kochian, L.V., 2010. Transcriptional regulation of metal transport genes and mineral nutrition during acclimatization to cadmium and zinc in the Cd/Zn hyperaccumulator, *Thlaspi caerulescence* (Ganges population). New Phyt. 185, 114-129. https://doi.org/10.1111/j.1469-8137.2009.03051.x.

Laurette, J., Larue, C., Llorens, I., Jaillard, D., Jouneau, P.-H., Bourguignon, J., Carrière, M., 2012. Speciation of uranium in plants upon root accumulation and root-to-shoot translocation: a XAS and TEM study. Environ. Exp. Bot. 77, 87-95. https://doi.org/10.1016/j.envexpbot.2011.11.005.

Lin, C., Kadono, T., Yoshizuka, K., Furuichi, T., Kawano, T., 2006. Effects of fifteen rare-earth metals on Ca^{2+} iInflux in tobacco cells. Z. Naturforsch. C J. Biosci. 61, 74-80. https://doi.org/10.1515/znc-2006-1-214.

Linsmaier, E.M., Skoog, F., 1965. Organic growth factor requirements of tobacco tissue cultures. Physiol. Plant. 18, 100-127. https://doi.org/10.1111/j.1399-3054.1965.tb06874.x.

Lopez-Fernandez, M., Moll, H., Merroun, M.L., 2019. Reversible pH-dependent curium(III) biosorption by the bentonite yeast isolate *Rhodotorula mucilaginosa* BII-R8. J. Hazard. Mater. 370, 156–163. https://doi.org/10.1016/j.jhazmat.2018.06.054.

Lütke, L., 2013. Interaction of selected Actinides (U, Cm) with Bacteria relevant to Nuclear Waste Disposal. Doctoral thesis TU Dresden, Germany.

Martinez-Gomez, N.C., Vu, H.N., Skovran, E., 2016. Lanthanide chemistry: from coordination in chemical complexes shaping our technology to coordination in enzymes shaping bacterial metabolism. Inorg. Chem. 55, 10083-10089. https://doi.org/10.1021/acs.inorgchem.6b00919.

Ménétrier, F., Taylor, D.M., Comte, A., 2008. The biokinetics and radiotoxicology of curium: a comparison with americium. Appl. Rad. Isot. 66, 632–647. https://doi.org/10.1016/j.apradiso.2007.12.002.

Moll, H., Stumpf, Th., Merroun, M., Rossberg, A., Selenska-Pobell, S., Bernhard, G., 2004. Time-resolved laser fluorescence spectroscopy study on the interaction of Cm(III) with *Desulfovibrio äspöensis* DSM 10631^{T}. Environ. Sci. Technol. 38, 1455–1459. https://doi.org/10.1021/es0301166.

Moll, H., Glorius, M., Barkleit, A., Rossberg, A., Bernhard, G., 2009. The mobilization of actinides by microbial ligands taking into consideration the final storage of nuclear waste: interactions of selected actinides U(VI), Cm(III), and Np(V) with pyoverdins secreted by *Pseudomonas fluorescens* and related model compounds. Wissenschaftlich-Technische Berichte, FZD-522. Dresden, Germany: Forschungszentrum Dresden-Rossendorf.

Moll, H., Lütke, L., Barkleit, A., Bernhard, G., 2013. Curium(III) speciation studies with cells of a groundwater strain of *Pseudomonas fluorescens*. Geomicrobiol. J. 30, 337–346. https://doi.org/10.1080/01490451.2012.688927.

Moll, H., Lütke, L., Bachvarova, V., Cherkouk, A., Selenska-Pobell, S., Bernhard, G., 2014. Interactions of the Mont Terri Opalinus Clay isolate *Sporomusa* sp. MT-2.99 with curium (III) and europium (III). Geomicrobiol. J. 31, 682-696. https://doi.org/10.1080/01490451.2014.889975.

Moll, H., Sachs, S., Geipel, G., 2020a. Plant cell (*Brassica napus*) response to europium(III) and uranium(VI) exposure. Environ. Sci. Pollut. Res. 27, 32048-32061. https://doi.org/10.1007/s11356-020-09525-2.

Moll, H., Lehmann, F., Raff, J., 2020b. Interaction of curium(III) with surface-layer proteins from *Lysinibacillus sphaericus* JG-A12. Colloids Surf. B: Biointerfaces 190. https://doi.org/10.1016/j.colsurfb.2020.110950.

Ozaki, T., Arisaka, M., Kimura, T., Francis, A.J., Yoshida, Z., 2002. Empirical method for prediction of the coordination environment of Eu(III) by time-resolved laser-induced fluorescence spectroscopy. Anal. Bioanal. Chem. 374, 1101–1104. https://doi.org/10.1007/s00216-002-1587-1.

Ozaki, T., Kimura, T., Ohnuki, T., Francis, A.J., 2005. Associations of Eu(III) with gram-negative bacteria, *Alcaligenes faecalis*, *Shewanella putrefaciens*, and *Paracoccus denitrificans*. J. Nucl. Radiochem. Sci. 6, 73-76. https://doi.org/10.14494/jnrs2000.6.73.

Rajabi, F., Jessat, J., Garimella, J.N., Bok, F., Steudtner, R., Stumpf, Th., Sachs, S., 2021. Uranium(VI) toxicity in tobacco BY-2 cell suspension culture. Ecotoxicol. Environ. Saf. 211, 111883. https://doi.org/10.1016/j.ecoenv.2020.111883.

Rossberg, A., Reich, T., Bernhard, G., 2003. Complexation of uranium(VI) with protocatechuic acid – application of iterative transformation factor analysis to EXAFS spectroscopy. Anal. Bioanal. Chem. 376, 631–638. https://doi.org/10.1007/s00216-003-1963-5.

Sachs, S., Heller, A., Weiss, S., Bok, F., Bernhard, G., 2015. Interaction of Eu(III) with mammalian cells: cytotoxicity, uptake, and speciation as a function of Eu(III) concentration and nutrient composition. Toxicol. In Vitro 29, 1555-1568. https://doi.org/10.1016/j.tiv.2015.06.006.

Sachs, S., Geipel, G., Bok, F., Oertel, J., Fahmy, K., 2017. Calorimetrically determined U(VI) toxicity in *Brassica napus* correlates with oxidoreductase activity and U(VI) speciation. Eviron. Sci. Technol. 51, 10843-10849. https://doi.org/10.1021/acs.est.7b02564.

Schläfer, H.L., Kling, O., 1956. Bedeutung isosbestischer Punkte für die spektrophotometrische Untersuchung chemischer Zeitreaktionen und Gleichgewichte. Angew. Chem. 68, 667-670. https://doi.org/10.1002/ange.19560682103.

Schmidt, M., Stumpf, T., Marques Fernandes, M., Walther, C., Fanghänel, Th., 2008. Charge compensation in solid solutions. Angew. Chem. Int. Ed. 47, 5846 –5850. https://doi.org/10.1002/anie.200705827.

Schreckhise, R.G., Cline, J.F., 1980. Comparative uptake and distribution of plutonium, americium, curium and neptunium in four plant species. Health Phys. 38, 817-824. doi: 10.1097/00004032-198005000-00009.

Schulz, R.K., Ruggieri, M.R., 1981. Uptake and translocation of neptunium-237, plutonium-238, plutonium-239, 240, americium-241, and curium-244 by a wheat crop. Soil Sci. 132, 77-82. https://doi.org/10.1097/00010694-198107000-00011.

Sharma, S., Singh, B., Manchanda, V.K., 2015. Phytoremediation: role of terrestrial plants and aquatic macrophytes in the remediation of radionuclides and heavy metal contaminated soil and water. Environ. Sci. Pollut. Res. 22, 946–962. https://doi.org/10.1007/s11356-014-3635-8.

Thakur, P., Ward, A.L., 2019. Sources and distribution of ^{241}Am in the vicinity of a deep geologic repository. Environ. Sci. Pollut. Res. 26, 2328–2344. https://doi.org/10.1007/s11356-018-3712-5.

Vanhoudt, N., Vandenhove, H., Horemans, N., Wannijn, J., Bujanic, A., Vangronsveld, J., Cuypers, A., 2010. Study of the oxidative stress related responses induced in *Arabidopsis thaliana* following mixed exposure to uranium and cadmium. Plant Physiol. Biochem. 48, 879-886. https://doi.org/10.1016/j.plaphy.2010.08.005.

Wang, L., Cheng, M., Chua, Y., Li, X., Chen, D.D.Y., Huang, X., Zhou, Q., 2016. Responses of plant calmodulin to endocytosis induced by rare earth elements. Chemosphere 154, 408-415. https://doi.org/10.1016/j.chemosphere.2016.03.106.

Wang, L.H., Li, J.G., Zhou, Q., Yang, G.M., Ding, X.L., Li, X.D., Cai, C.X., Zhang, Z., Wei, H.Y., Lu, T.H., Deng, X.W., Huang, X.H., 2014. Rare earth elements activate endocytosis in plant cells. Proceedings of the National Academy of Sciences of the United States of America 111, 12936-12941.

Wolter, J.-M., Schmeide, K., Huittinen, N., Stumpf, Th., 2019. Cm(III) retention by calcium silicate hydrate (C-S-H) gel and secondary alteration phases in carbonate solutions with high ionic strength: a site-selective TRLFS study. Sci. Rep. 9, 14255. https://doi.org/10.1038/s41598-019-50402-.

Xiao, B., Lösch, H., Huittinen, N., Schmidt, M., 2018. Local structural effects of Eu^{3+} incorporation into xenotime-type solid solutions with different host cations. Chem. Eur. J. 24, 13368-13377. https://doi.org/10.1002/chem.201802841.

S. Yamasaki, S., Shirai, O., Kano, K., Kozai, N., Sakamoto, F., Ohnuki, T., 2013. Adsorption behavior of lanthanide ions on nonbiological phospholipid membranes: a model study using liposome. Chem. Lett., 42, 819-821. https://doi.org/10.1246/cl.130226.

Yang, Q., Wang, L., Zhou, Q., Huang, X., 2015. Toxic effects of heavy metal terbium ion on the composition and functions of cell membrane in horseradish roots. Ecotoxicol. Environ. Saf. 111, 48-58. https://doi.org/10.1016/j.ecoenv.2014.10.002.

Yang, Q., Wang, L., He, J., Yang, Z., Huang, X., 2018. Direct imaging of how lanthanides break the normal evolution of plants. J. Inorg. Biochem. 182, 158-169. https://doi.org/10.1016/j.jinorgbio.2018.01.020.

Zagoskina, N.V., Goncharuk, E.A., Alyavina, A.K., 2007. Effect of cadmium on the phenolic compounds formation in the callus cultures derived from various organs of the tea plant. Russ. J. Plant Physiol. 54, 237-243. https://doi.org/10.1134/S1021443707020124.